# **Building-road Collaborative Extraction from Remotely Sensed**

# **Images via Cross-Interaction**

Haonan Guo<sup>1</sup>, Xin Su<sup>2\*</sup>, Chen Wu<sup>1</sup>, Bo Du<sup>3,4,5</sup>, Liangpei Zhang<sup>1</sup>

- 1 State Key Laboratory of Information Engineering in Surveying, Mapping and Remote Sensing, Wuhan University, Wuhan, China
- 2 School of Remote Sensing and Information Engineering, Wuhan University, Wuhan, China
- 3 National Engineering Research Center for Multimedia Software, Wuhan University, Wuhan, China
- 4 Institute of Artificial Intelligence, Wuhan University, Wuhan, China
- 5 School of Computer Science, Wuhan University, Wuhan, China

# **Abstract**

Buildings are the basic carrier of social production and human life; roads are the links that interconnect social networks. Building and road information has important application value in the frontier fields of regional coordinated development, disaster prevention, auto-driving, etc. Mapping buildings and roads from very high-resolution (VHR) remote sensing images have become a hot research topic. However, the existing methods often ignore the strong spatial correlation between roads and buildings and extract them in isolation. To fully utilize the complementary advantages between buildings and roads, we propose a building-road collaborative extraction method based on multi-task and cross-scale feature interaction to improve the accuracy of both tasks in a complementary way. A multi-task interaction module is proposed to interact information across tasks and preserve the unique information of each task, which tackle the 'seesaw phenomenon' in multitask learning. By considering the variation in appearance and structure between buildings and roads, a cross-scale interaction module is designed to automatically learn the optimal reception field for different tasks. Compared with many existing methods that train each task individually, the proposed collaborative extraction method can utilize the complementary advantages between buildings and roads by the proposed

inter-task and inter-scale feature interactions, and automatically select the optimal reception field for different tasks. Experiments on a wide range of urban and rural scenarios show that the proposed algorithm can achieve building-road extraction with outstanding performance and

efficiency.

**Keywords:** Building extraction, road segmentation, multitask learning, deep learning.

1. Introduction

Buildings and roads are the two most basic man-made elements of our society. To be specific, buildings are basic carriers for social production and human life, while roads interconnect

social network that enables goods and information transportation(Fleischmann and Arribas-

Bel, 2022; Laurance et al., 2014). The geodata of buildings and roads are valuable for

understanding human activities and thus boost the sustainable development goals(SGD)

including coordinated regional development, sustainable urban planning, public health, disaster

risk reduction, etc.(Crew, 2021). Furthermore, the geoinformation of buildings and roads is

indispensable for frontier applications such as autonomous driving and smart cities(LI et al.,

2013).

The very high-resolution (VHR) remote sensing imaging technique provides abundant image data sources for mapping buildings and roads in large areas. Traditionally, these building and

road maps are produced by visual interpreting, manual labeling, and surveying(Griffiths and

Boehm, 2019). Despite its high accuracy, manually producing such geodata is time-consuming,

especially for citywide or nationwide mapping(Huang et al., 2020). Moreover, it cannot meet

the requirements of the up-to-date databases from many geodata-oriented applications such as

autonomous driving, since regular manual updating is laborious in the long run(Guo et al.,

2021b). To this end, many studies have attempted to design automatic methods for mapping

buildings and roads from VHR remote sensing images. Over the past decades, mainstream

2

building and road extraction algorithms have developed from handcrafted feature-based methods to deep learning-based methods(Zhu et al., 2017). The traditional handcrafted-based methods seek to select spatial-spectral features that can well distinguish objects of interest from the background(Awrangjeb et al., 2013; Ghanea et al., 2016; Huang and Zhang, 2011; Zha et al., 2003). However, limited by expert knowledge and feature generalization, it is time-consuming to manually design optimal feature descriptors or classifiers that can be generalized to large areas.

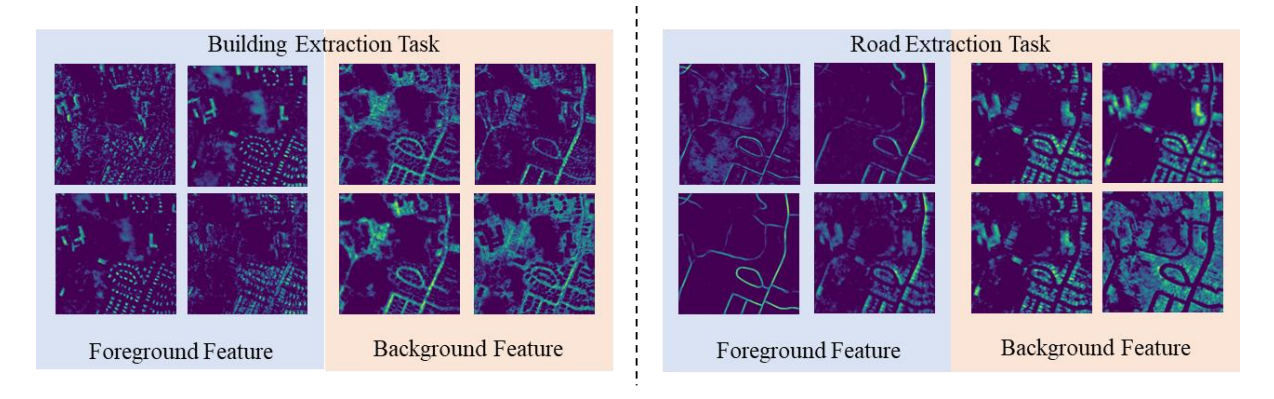


**Figure 1.** The illustration of the output features of U-Net models that are trained individually on building extraction and road extraction tasks. Buildings and roads are complementary in the feature space.

The convolution neural networks (CNN) of deep learning can automatically learn image descriptors and extract optimal features through backpropagation(Long et al., 2015), and thus have been proven more effective than the handcrafted feature-based methods(Guo et al., 2021a). Many studies have designed new CNN structures to improve the models' performance on buildings or roads(Guo et al., 2021c; Lu et al., 2019; Xu et al., 2018). However, despite the pivotal role that buildings and roads have in human society, many prevailing algorithms extract buildings or roads in isolation(Ayala et al., 2021b; Zhang and Wang, 2019), and ignore the strong spatial correlation relation between buildings and roads. In our experiments, we empirically find that the strong correlation relation exists not only in the real-world space but also in the feature space. In Figure 1, we visualize the deep features extracted by building extraction models and road extraction models using the U-Net architecture(Ronneberger et al.,

2015). An interesting finding is that the building extraction model learns to localize road regions other than building areas even without any supervision from the road areas since the model is trained only with the building ground truth. Similarly, the road segmentation model learns the building information automatically with supervision from the building ground truths. Since these image descriptors of CNNs are optimized through backpropagation(Krizhevsky et al., 2017), the model's focus on background features demonstrates the correlation relationship of buildings and roads in the feature space. It also implies that the building extraction and road extraction tasks can improve both tasks' accuracy in a collaborative way.

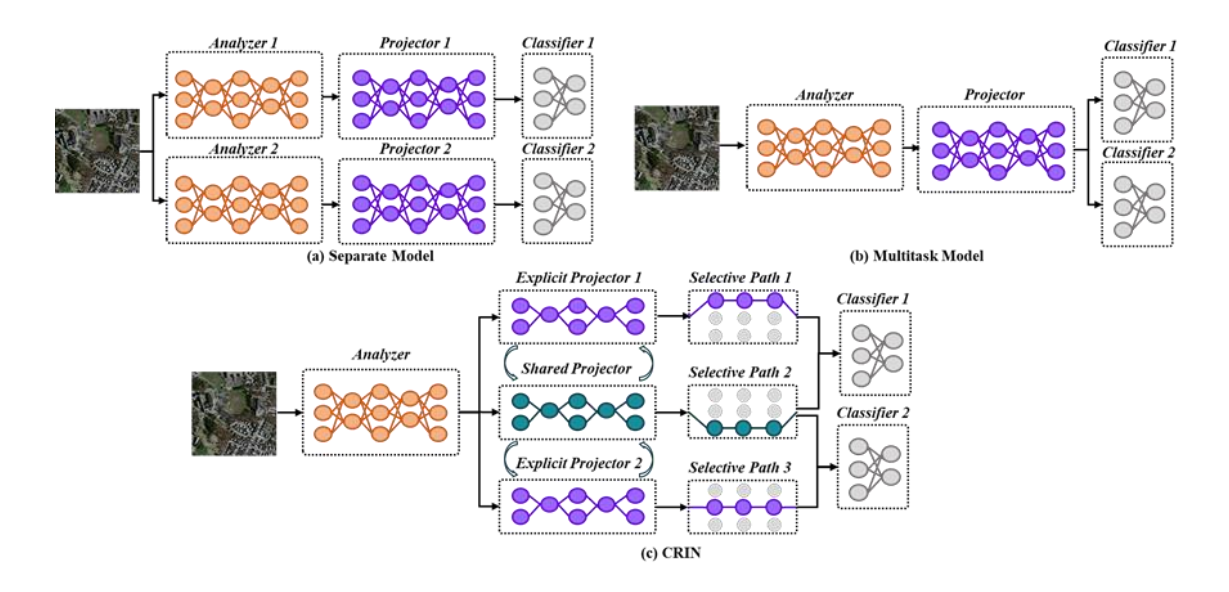


**Figure2.** The comparison among different architectures for building-road collaborative extraction, including (a) separate models trained individually for different tasks (b) multitask model that predicts building and road using multiple classifiers, and (c) our proposed Cross-Interaction (CRIN) architecture that embeds task-shared and task-specific feature spaces and selective paths.

However, although some existing methods attempted to design unified network architecture for building and road extraction, these models are trained independently on each task and do not consider the complementary relation between buildings and roads, as shown in Figure 2 (a) (Ayala et al., 2021b; Zhang and Wang, 2019). To address this problem, an intuitive question is "can we design a single multitask model for simultaneously extracting buildings and roads?". Some studies have introduced multitask networks by embedding two classifiers to predict buildings and roads from the extracted features, as depicted in Figure 2(b)(Abdollahi et al.,

2021; Alshehhi et al., 2017; Ding et al., 2021). However, these multitask network designs lead to the common multitask learning issue of the "seesaw phenomenon" that the accuracy of one task is often improved by hurting the performance of another task(Tang et al., 2020), which is also demonstrated in our experiment. Moreover, these methods extract building and road features using a unified network architecture and do not consider the different requirements of models' reception fields between different tasks, which may also deteriorate multitask feature representation.

To address these problems, we propose a CRoss-INteraction (CRIN) model with a novel feature space design. As shown in Figure 2(c), CRIN separates the common feature space into task-specific and task-shared feature spaces and utilizes a progressive grouping scheme to realize inner-task and cross-task feature interaction, improving task-specific and task-shared feature representations. Moreover, as the optimal reception field of the different tasks varies, a cross-scale interaction module is designed to automatically learn and select the optimal reception field for each feature space, and thus exploit optimal feature representations for each specific task. The proposed CRIN model can boost the performance of both building extraction and road extraction tasks in a complementary way. Our main contributions are summarized as follows:

- 1. A multitask interaction module is proposed to take advantage of the complement of spatial correlation relationship between buildings and roads. The proposed model can achieve crosstask interactions within the shared feature space while preserving the unique feature space of each task under the inner-task interaction design. It alleviates the problem of isolated or unbalanced learning as proposed by the existing methods.
- 2. Since the building extraction and road extraction tasks depend on the model's reception field differently, a cross-scale interactive perception module is designed. The module

adaptively determines the optimal receptive field for each task through back-propagation, and thus improves the collaborative representation of building and road features.

3. Extensive experiments on a wide range of urban and rural scenes across different cities and states demonstrate the effectiveness of the method, which achieves the highest accuracy in building and road extraction tasks. In comparison to the unified network structures that are trained separately or the multitask structures that cause the 'seesaw phenomenon', the proposed CRIN model takes advantage of the complementary advantages between buildings and roads and achieves the best performance and efficiency.

### 2. Related Works

# 2.1 Building Extraction

Extracting buildings from VHR remote sensing images has long been a challenging task due to the high inner-class variation and small inter-class variation of VHR remote sensing images(Guo et al., 2021a). For example, non-building features with similar colors, shadows from nearby objects, and heterogeneity of roofs are some major problems that hinder the process of automation(Ghanea et al., 2016). To overcome the confusion from non-building features, early methods seek to select features that can well represent buildings, and design multiple criteria to discriminate buildings from complex backgrounds. For example, Bouziani et al. integrate color and geometric features into building extraction(Bouziani et al., 2010). Ok et al. introduce the shadow feature as evidence of building regions, and apply the GrabCut algorithm to extract building regions from remote sensing images(Ok et al., 2013). Huang and Zhang introduce morphological features and shadow features for automatic building extraction(Huang and Zhang, 2011). These criteria, however, are designed and tuned manually for promising performance in the study areas, which are hard to be applied to large-scale applications in practical scenarios (Adriano et al., 2021).

In recent years, some studies introduced data-driven deep-learning techniques to the building extraction field. The advantage of deep learning is that it can automatically learn feature representation from the input image and make classifications in an end-to-end manner(Long et al., 2015). Many works have been proposed to improve the fully convolutional networks(FCN) for building extraction. The main direction of improvements lies in building boundary refinement(Bai et al., 2022; Liu et al., 2021; Shao et al., 2020), multiscale feature fusion(Ji et al., 2019; Zhu et al., 2020), and dilated convolution(Guo et al., 2021a; Liu et al., 2018). Although much effort has been made, the automation for large-scale building footprint mapping is still a challenging task.

# 2.2 Road segmentation

Extracting roads from remote sensing images is also challenging due to diverse road materials and complex backgrounds(Lian et al., 2020). Since roads are stripe-shape objects with multiple intersections, spatial features such as geometric(Seppke et al., 2016), topological(Huang and Zhang, 2009), and texture(Yager and Sowmya, 2003) features are widely used in the handcrafted feature-based methods. Similar to building extraction, the traditional handcrafted feature-based methods show limited performance when applied to large areas. The data-driven learning-based have shown better performance and generalization than tradition methods. Due to the distinctive shape characteristic of roads, traditional convolutional layers of small kernel size cannot well capture the shape information, and a mainstream of research focus is to enlarge the models' reception field to capture road information(Lian et al., 2020). For example, D-LinkNet introduces multiple branches of dilated convolutional layers to capture features at different scales(Zhou et al., 2018). Lu et al. introduced a globally aware network to perceive long-range information at each decoder stage(Lu et al., 2021). Belli et al. introduced a self-attention module to capture enhance global context representation by capturing long-range similarity(Belli and Kipf, 2019). Since roads vary in width and materials,

they rely on different levels of model reception fields. It is challenging to design a model that can completely extract varied roads from complex backgrounds.

# 2.3 Building-road extraction

The existing building-road extraction methods can be categorized into unified structurebased and multitask networks. The unified structure-based methods aim to design a unified network by considering the characteristic of buildings and roads. For example, Zhang and Wang proposed a unified network structure(Zhang and Wang, 2019) with a large model reception field for building and road extraction. Ayala et al. introduced Res-U-Net to extract buildings and roads using crowdsource data as the training set(Ayala et al., 2021b). Saito et al. proposed unified U-Net architectures embedded with recurrent neural networks and dense connections for building and road extraction(Saito et al., 2016). These unified structures, however, do not consider the spatial correlation relation between buildings and roads. Moreover, these models are trained separately on different tasks, and thus double the computational burden since the image should pass through the model twice to generate building and road predictions. To this end, some studies designed multitask networks to predict the building and road in a single network. For example, some studies transmit the binary classification method into the multiclass classification method and classify the image patches into buildings, roads, and backgrounds (Alshehhi et al., 2017; Mnih and Volodymyr, n.d.; Saito et al., 2016). These patch-based methods do not utilize the global context information and are prone to cause large building misclassification and road disconnection due to insufficient spatial semantics(Saito et al., 2016). Some further studies introduce FCN to extract buildings and roads in a single model. Ding et al. proposed a non-local feature search network (Ding et al., 2021) embed with a self-attention module to strengthen feature representation. Ayala et al. (Ayala et al., 2021a) designed multitask strategies to train each category against the background before and fuse the predictions using post-processing. There are two major issues that hinder the performance of the building-road extraction, including 1. many existing multitask learning schemes directly attach several classifiers to generate multi-predictions, which may lead to the 'seesaw phenomenon' that features of one task becomes dominant and sacrifice the performance of the other task, and 2. The model reception fields for building and road extraction tasks are unified, ignoring the different requirements of model reception fields for different tasks. In this paper, we overcome these shortcomings by separating the common feature space into task-specific feature and task-shared future spaces with inner-task and cross-task feature interaction. A cross-scale interaction module then is designed to automatically learn and select the optimal reception filed for each feature spaces.

# 3. Methodology

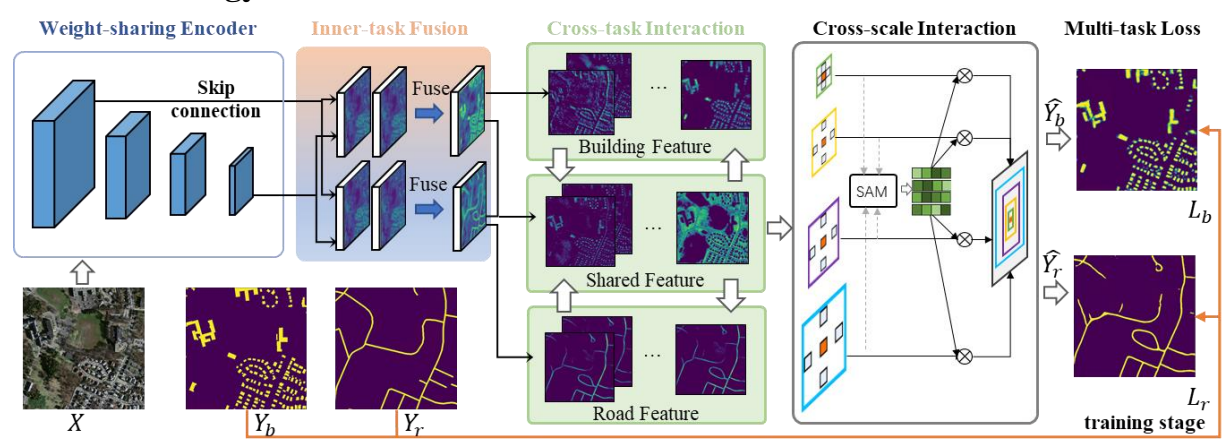


**Figure3.** The flowchart of the proposed Cross-Interaction (CRIN) network, which includes a weight-sharing encoder network, a multitask interaction module (MFI) that enables inner-task and cross-task feature interaction, and a cross-scale interaction module (CSI) to select and integrate optimal feature scales.

### 3.1 Overview

To take advantage of the correlation relationship between buildings and roads, we propose a CRoss-INteraction (CRIN) network to realize the simultaneous extraction of buildings and roads in a single network. As shown in Figure 3, CRIN takes the VHR remote sensing images as the input and outputs the prediction of building and road maps simultaneously to improve learning efficiency through information sharing between tasks. Following the encoder-decoder

design, the input images are first fed into the encoder network for hierarchical feature extraction. The extracted features are then copied and transmitted to the decoder network to refine feature resolution and generate building and road extraction. In each decoder stage, a multitask feature interaction (MFI) module is designed to address the 'seesaw phenomenon' that deteriorates multitask learning, which includes the inner-task fusion stage and the cross-task interaction stage. MFI performs inner-task feature fusion to integrate useful information coming from the encoder network; a cross-task interaction scheme then separates the feature space into task-specific and task-shared feature spaces for better feature interaction. In the task-specific feature space, the features are expected to learn representations that are optimal for the specific task, while the features of both tasks interact in the shared feature space. As a result, MFI is able to preserve the features of each specific task and take advantage of the complementary between building features and road features. Furthermore, a cross-scale interaction (CSI) module is integrated after MFI to select the optimal feature scale for each task, since different objects of interest rely on the reception field differently. Finally, the model is optimized with the building and road ground truths to handle the practical challenges of joint learning.

# 3.2 Multi-task interaction module

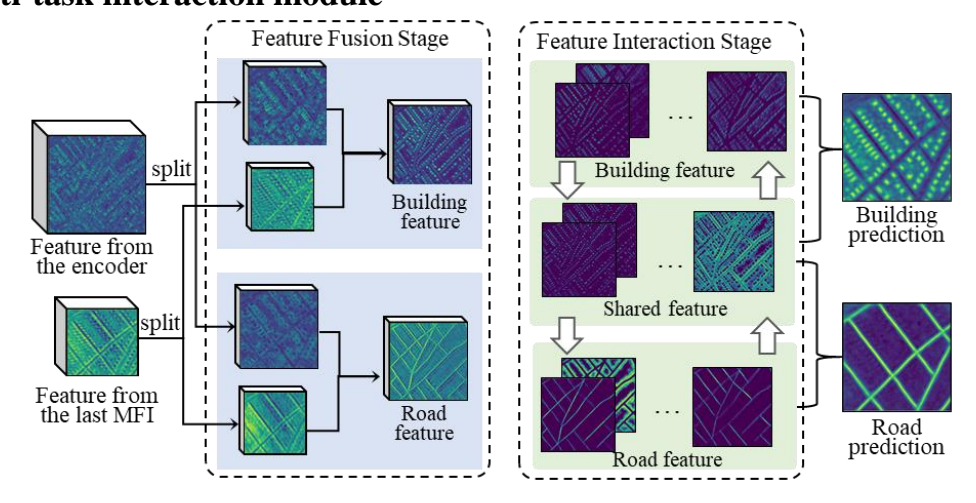


Figure 4. The architecture of the multi-task interaction (MTI) module.

Motivated by the strong spatial correlation relationship between buildings and roads, we expect to train a model that utilizes the complementary advantages between buildings and roads

and outperforms the single-task model that is trained separately. We propose a multi-task interaction (MTI) module to fully utilize the complementary advantage between buildings and roads. As shown in Figure 4, the proposed MFI tasks the output features from the last decoder stage and shallow features transmitted from the encoder network as the input. Deep features are rich in contextual semantics, but their edge details are insufficient due to low spatial resolution. On the contrary, features extracted by shallow encoder convolutional layers contain rich edge details of the whole image other than the objects of interest. In conventional decoder design, the common is to concatenate the multiple features and fuse them using a single convolutional feature. Another convolutional layer then refines the features and outputs the feature to the next decoder stage. However, in the multitask learning scheme, directly concatenating and convoluting multiple features into a unified representation leads to the 'seesaw phenomenon' that the features of one task become dominant and sacrifice the performance of the other task(Tang et al., 2020).

To address this problem, we aim to separate the unified feature space to ensure a proper learning space for each task, which also allows information sharing. The proposed MTI module includes the feature fusion stage and the feature interaction stage, as illustrated in Figure 4. In the fusion stage, we guide the model fuse building features and road features separately, since different tasks focus on different details contained in the input feature. We split the input features into two groups and concatenate features from each group in alternation. Convolution with a group size of two is performed to the concatenated features to generate building features and road features that contain rich semantic and spatial details. In this way, features from each feature space can focus on refining the spatial details of the specific task. The real-world example in Figure 4 shows that the fusion result of each task can better locate building and road regions compared with the input feature. The features are then projected for cross-task interaction in the interaction stage.

In the interaction stage, we further project the features into the task-specific feature spaces, including the building feature space and the road feature space, and a task-shared feature space that enables cross-task feature interaction. In this way, features of both tasks can interact in the shared feature space, and task-specific features can be preserved in the task-specific feature space.

We then explain why MFI is a lightweight and effective decoder design for building-road collaborative extraction. If we directly adopt the conventional U-Net decoder for collaborative extraction, one task may become dominant in the training process, and the features cannot be well balanced between different tasks(Tang et al., 2020). However, in MFI, we separate the decoder into the feature fusion stage and the feature interaction stage, where the former is responsible for fusing the features for each task and the latter is capable of information interaction across the different tasks. Moreover, MFI can be implemented by successive feature splitting and group convolutions, which saves one-third of the computational cost as compared with the conventional decoders in theory. It demonstrates that MFI is an effective and lightweight decoder module for building-road collaborative segmentation.

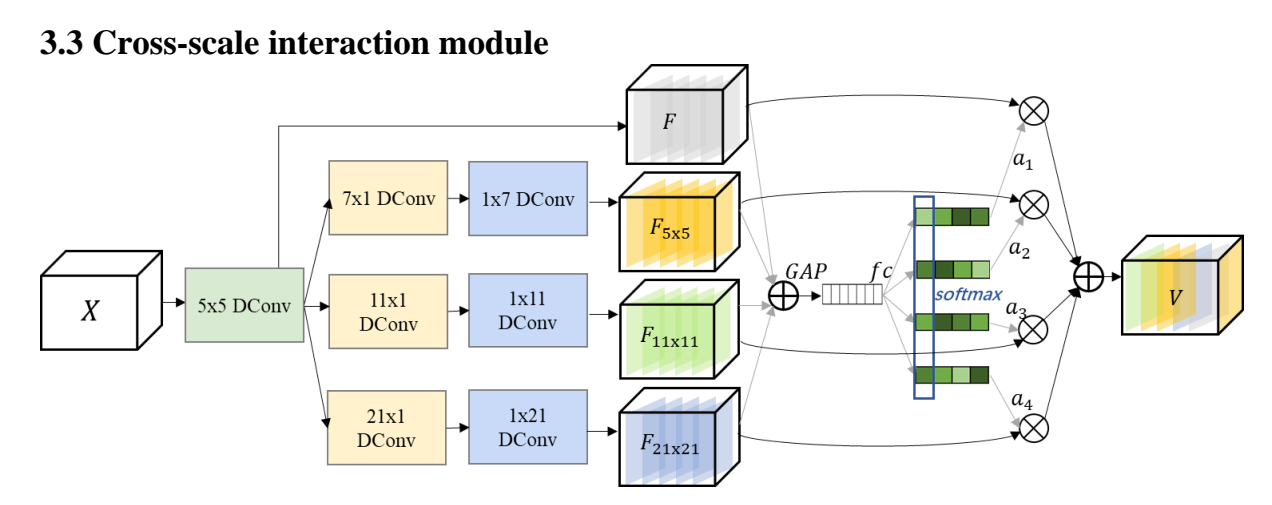


Figure 5. The architecture of the cross-scale interaction (CSI) module.

MFI separates task-specific and task-shared features explicitly, and thus preserves the feature space of each task and allows cross-task feature interaction. As depicted in Figure 5,

CSI contains multiple branches of different large convolutional kernels, which refer to different scales of the reception field. Large kernel sizes with depthwise convolutional layers have been proven effective in improving the model's reception field. However, since the optimal reception field for different tasks varied, manually selecting a scale of large kernel size may not be helpful in improving multitask accuracy. To address this problem, the input features are fed into multiple branches of different large convolutional kernels and introduce a selective kernel mechanism to determine the contribution of each scale. Moreover, to alleviate the heavy computational burden of multiple large-kernel branches, we introduce alternative row-wise convolution and column-wise convolution, which effectively reduces the computational cost and improves the receptive field of the model.

Specifically, CSI takes the output feature f of MTI as the input. f is firstly fed into a depthwise convolutional layer of kernel size of 5x5 to extract the initial feature  $f_{init}$ :

$$f_{init} = DConv_{5x5}(f) \tag{1}$$

in which DConv<sub>ixj</sub>(·) represents a depthwise convolutional layer of kernel size ixj. Then f<sub>init</sub> is passed through 4 branches including the reception field of 7x7, 11x11, 21x21, and the residual branch that maintains the original reception field. Moreover, if we directly feed the features into convolution layers of kernel size kxk, the model's parameters increase exponentially. For example, the parameters of a convolution layer of 21x21 kernel size are 49 times that of the 3x3 kernels. Inspired by the inception module, we apply column-wise and row-wise convolution in success to increase the model reception field with less computational cost. The computation process of these branches is as follows.

$$f_{7x7} = \text{Conv}_{1x7}(\text{Conv}_{7x1}(f_{init})) \tag{2}$$

$$f_{11x11} = Conv_{1x11}(Conv_{11x1}(f_{init}))$$
 (3)

$$f_{21x21} = Conv_{1x21}(Conv_{21x1}(f_{init})$$

$$\tag{4}$$

$$f_{\text{skip}} = f_{init} \tag{5}$$

Given the features of different reception fields, the next step is to decide the contribution of each branch, which is the key step in determining the optimal scale for each task. We introduce a scale attention module to predict the contribution of each scale. Features of all scales are summed pointwise, followed by a global average pooling module that aggregates global context information of all scales. A multilayer perceptual layer is connected to generate a vector of shape 4xC, followed by a softmax operation that converts the output into scale attention values, where 4 represents the attention value of each scale. This contribution value is then multiplied by the features of each scale along the channel axis. The final output of CSI is the summation of all the attention-activated features:

$$f_{fuse} = GAP(f_{7x7}) + GAP(f_{11x11}) + GAP(f_{21x21}) + GAP(f_{init})$$
 (6)

$$Attn = softmax(MLP(f_{fuse})) \tag{7}$$

$$f_{out} = Attn_1 \cdot f_{7x7} + Attn_2 \cdot f_{11x11} + Attn_3 \cdot f_{21x21} + Attn_4 \cdot f_{init}, where \ \Sigma_i^{i=4} \ Attn_i = 1 \eqno(8)$$

We then explain why CSI is capable of learning the optimal scale for different tasks. Since we adopted depthwise convolution in the multi-branch stages and the scale attention stage, the optimal scale for different feature layers is learned independently. It means that features from different tasks can automatically learn the contribution of each scale without inference from the other task. Compared with many existing works that design a unified framework for buildings and roads in ignorant of different requirements of the reception field, CSI can automatically determine the optimal scale of each task and extract features with the optimal reception field. Another advantage of CSI is that it is a super lightweight module that can effectively improve the reception field for different tasks. By introducing depthwise 1xn and

nx1 convolutions in succession, the computation burden is reduced to 1/600 compared with CSI without these improvements.

### 3.4 Model Details

The CRIN model is implemented under the deep learning framework of Pytorch and is optimized using the AdamW optimizer(Kingma and Ba, 2017). The learning rate is set to 0.001 initially and is adjusted under the 'poly' scheduler with power 0.9. The model is trained for 40k iterations with a batch size of 16. To avoid overfitting, we adopted a data augmentation strategy that randomly rotates, flips, and scales the input image and label patches. The loss function of CRIN includes three parts, the building supervision loss, the road supervision loss, and the deep supervision loss. The building supervision loss and the road supervision loss are the summations of cross entropy loss and dice loss between the building and road prediction  $\widehat{y_b}$ ,  $\widehat{y_r}$  and their corresponding ground truths  $y_b$  and  $y_r$ :

$$L_{building} = (\text{Dice}(\widehat{y_b}, y_b) + \text{CE}(\widehat{y_b}, y_b))/2 \tag{9}$$

$$L_{road} = (\operatorname{Dice}(\widehat{y_r}, y_r) + \operatorname{CE}(\widehat{y_r}, y_r))/2 \tag{10}$$

We also introduce the deep supervision loss to guide the model to learn task-specific and task-shared features. Given the task-specific building feature  $f_b$ , road feature  $f_r$ , and the task-shared feature  $f_s$ , we apply deep supervision to generate deep building and road predictions from these features. Specifically, the prediction of each task is generated by the task-specific feature and task-shared feature:

$$L_{aux} = \sum_{i=1}^{n} \text{CE}(Conv_{1x1}([f_b^i, f_s^i]), y_b) + \text{CE}(Conv_{1x1}([f_r^i, f_s^i]), y_r)$$
(11)

In this way, features from task-specific feature space are able to learn information that is helpful to the specific task, and the task-shared features are able to learn common feature that is beneficial to both tasks. The overall loss is the weighted summation of the building supervision loss, the road supervision loss, and the deep supervision loss. Since the deep

supervision loss is the auxiliary loss that guides model learning, we adopted a weight of 0.1 to  $L_{aux}$ , and the final loss function is calculated as follows:

$$L = L_{building} + L_{road} + 0.1 * L_{aux}$$
 (12)

After the model converges, the models' performance is evaluated on the test dataset using evaluation metrics including precision, recall, F1-score, and IoU. Furthermore, the efficiency of models also matters in large-scale mapping, since large models are usually more time-consuming than lightweight models. To this end, we also testify the number of parameters, Flops, and frame per second (FPS) of the model to validate the computational cost and inference speed of the methods.

# 4. Experiments and Analysis

# 4.1 Experiments Settings

### 4.1.1 Datasets

We select two large-scale building and road datasets to evaluate the performance of the proposed method.

- The Massachusetts dataset (Mnih and Volodymyr, n.d.): The Massachusetts building and road dataset is a large-scale dataset that covers a wide variety of urban and rural regions in Massachusetts. The building and road labels are generated by the OpenStreetMap (OSM) project. Each image has an image size of 1500x1500 with a spatial resolution of 1m. Following the data partition method in (Saito et al., 2016), we collect the patches that contain both building and road labels and obtain 137, 4, and 10 patches for training, validation, and testing, respectively. We clip the images and their corresponding building and road labels into 512x512 patches with a stride ratio of 0.5.
- The aerial imagery object identification dataset(Bradbury et al., 2016): The aerial imagery object identification(AIOI) dataset is a multi-city dataset, which contains 25

unique images from 9 different cities including urban and suburban areas. This dataset is suitable for evaluating the model's performance in large-scale and cross-city mapping. The image resolutions range from 0.15 to 0.3 meters; the ground truth labels are produced using OSM. The dataset includes images from suburban areas of 6 cities and urban areas from 3 cities. We randomly select New York, Atlanta, and New Heaven as the test dataset and the rest as the training dataset. The cross-city mapping of the AIOI dataset poses a great challenge to the generalization and performance of the models.

### 4.1.2 Evaluation metrics

The models' performance is evaluated by calculating the precision, recall, F1-score, and IoU between the model predictions and the ground truths. Precision represents the ratio of predicted foreground pixels that are correctly predicted; recall indicates the proportion of the ground truth buildings or roads that are correctly predicted; F1-score is the harmonic average between precision and recall. IoU denotes the intersection between prediction and ground truth over their union. These evaluation metrics can be calculated as follows.

$$Precision = \frac{TP}{TP + FP}$$
 (13)

$$Recall = \frac{TP}{TP + FN} \tag{14}$$

F1 Score = 
$$2 * \frac{Precision*Recall}{Precision+Recall}$$
 (15)

$$IoU = \frac{TP}{TP + FN + FP} \tag{16}$$

where TP, FP, and FN represent the number of true positive, false positive, and false negative pixels in the test dataset, respectively. Furthermore, the implementation speed and the computational cost of the model is important in large-scale mapping scenario, thus we evaluated the model complexity using three metrics including the amount of parameter, floating point operations (FLOPs), and frame per second (FPS). The parameter number reflects the model size; FLOPs denote the computational cost of the model; FPS corresponds to the inference speed of the model.

### **4.1.3 Comparison Methods**

We compare our proposed method with seven building-road collaborative extraction methods. These comparison methods can be categorized into separate methods(Abdollahi et al., 2021; Ayala et al., 2021b; Mnih and Volodymyr, n.d.; Zhang and Wang, 2019) and multitask methods(Alshehhi et al., 2017; Ding et al., 2021; Saito et al., 2016). The separate methods usually design a unified architecture for building and road extraction, which is trained on two tasks individually; the multitask methods introduce multiple classifiers or increase the output channel of classifiers to generate building and road predictions in a single model. We give a brief introduction to these methods as follows.

- ➤ Mnih and Volodymyr(Mnih and Volodymyr, n.d.) proposed a patch-based classification network to extract buildings and roads in separation. The patches of 64x64 pixels are cropped from the image and predict the category of the central patches of 16x16 pixels. The models are trained and inferred individually with building and road extraction tasks.
- Ayala et al.(Ayala et al., 2021b) proposed a modified version of U-Net using ResNet as the encoder network. This model is utilized to extract buildings and roads in separation. The predictions are merged after inferring the building and road predictions separately.
- Abdollahi et al.(Abdollahi et al., 2021) introduce novel mechanisms, including bidirectional LSTM, dense connection, and attention modules to improve the model performance on building and road extraction. The model is trained on building and road extraction tasks in separation. We select the reported best MCG-Net for comparison.
- ➤ JointNet(Zhang and Wang, 2019) is a unified and effective architecture for building and road extraction. The network combines atrous convolution with densely connected convolutions to enlarge the model reception field. The model is trained separately on building and road extraction tasks.

- Non-local feature search network(NFSNet) can extract buildings and roads in a single model that generates multiple channels in the output prediction(Ding et al., 2021). Self-attention modules and feature refinement modules are designed to alleviate building misjudgment and road disconnection problems.
- The method as proposed by Alshehhi et al. is a patch-based method for the simultaneous extraction of buildings and roads(Alshehhi et al., 2017). The category of the central 16x16 pixels is predicted from the surrounding 64x64 pixels. A post-processing method is introduced to alleviate the misclassification problem using superpixels.
- ➤ Saito et al. proposed a multiple object extraction method for building and road extraction(Saito et al., 2016). It is a patch-based method that introduced channel-wise inhibited softmax. The final prediction is generated patch-by-patch under model averaging.

# 4.2 Experiments on the Massachusetts dataset

We present the experimental results of the comparison methods in Table I, with the highest score marked in bold and the second highest score underlined. From Table I we can see that our proposed CRIN achieves the IoU and F1-score on both building and road extraction tasks. Although the method proposed by Alshehhi et al. performs well in the precision score, the recall score is rather low, indicating that many foreground pixels are omitted. CRIN outperforms the separate networks by utilizing the spatial correlation between buildings and roads, thus improves the accuracy of both tasks. Among the multitask methods, the methods as proposed by Saito et al. and Alshehhi et al. are the patch-based methods that cannot fully utilize the spatial details from VHR remote sensing images, since only the 64x64 patches are fed forward the model. The segmentation-based NFSNet, however, cannot perform well on the Massachusetts dataset since it generates predictions from features that obtain 1/16 of the image resolution, causing serious omission of tiny buildings

and roads. On the contrary, our proposed CRIN model is a multitask model that obtains accurate building and road extraction from remote sensing images.

Table 1 Quantitative Comparison with SOTA Methods on the Massachusetts dataset

| Method          | Type      | Task     | IoU   | Precision    | Recall | F1-Score |
|-----------------|-----------|----------|-------|--------------|--------|----------|
| CRIN(ours)      |           | Building | 71.15 | 83.79        | 82.5   | 83.14    |
| , ,             |           | Road     | 59.09 | <u>75.49</u> | 73.12  | 74.29    |
| Saito et al.    |           | Building | 64.17 | 80.64        | 75.86  | 78.17    |
|                 | Multitask | Road     | 53.47 | 73.26        | 66.43  | 69.68    |
| Alshehhi et al. |           | Building | 65.36 | 85.8         | 73.29  | 79.05    |
|                 |           | Road     | 56.27 | 82.98        | 63.61  | 72.02    |
| NFSNet          |           | Building | 59.11 | 76.14        | 72.56  | 74.3     |
|                 |           | Road     | 51.88 | 70.19        | 66.55  | 68.32    |
| JointNet        |           | Building | 69.38 | 85.52        | 78.61  | 81.92    |
|                 |           | Road     | 56.89 | 79.11        | 66.95  | 72.52    |
| MCG-UNet        |           | Building | 66.59 | 84.45        | 75.9   | 79.94    |
|                 | Separate  | Road     | 57.79 | 76.4         | 70.35  | 73.25    |
| Res-U-Net       | -         | Building | 67.44 | 78.88        | 82.31  | 80.56    |
|                 |           | Road     | 56.98 | 76.62        | 68.96  | 72.59    |
| Mnih et al.     |           | Building | 62.64 | 81.9         | 72.7   | 77.03    |
|                 |           | Road     | 53.22 | 75.95        | 64     | 69.47    |

We visualize some examples of the building and road predictions in Figure 6, where the green, blue, and red pixels represent the correctly predicted, the omitted, and the misclassified pixels. From Figure 6 rows 1-2, we can see that NFS-Net and the method proposed by Alshehhi et al. omitted some large-scale buildings nearby roads. However, CRIN can well preserve the integrity of the predicted buildings by considering the spatial correlation between buildings and roads. Moreover, as shown in Figure 6 rows 3-4, some tiny roads are misclassified or omitted by all the comparison methods, but CRIN can correctly predict the tiny roads by adaptively selecting the optimal reception field for perceiving the roads. CRIN is an effective model for simultaneously extracting buildings and roads from remote sensing images.

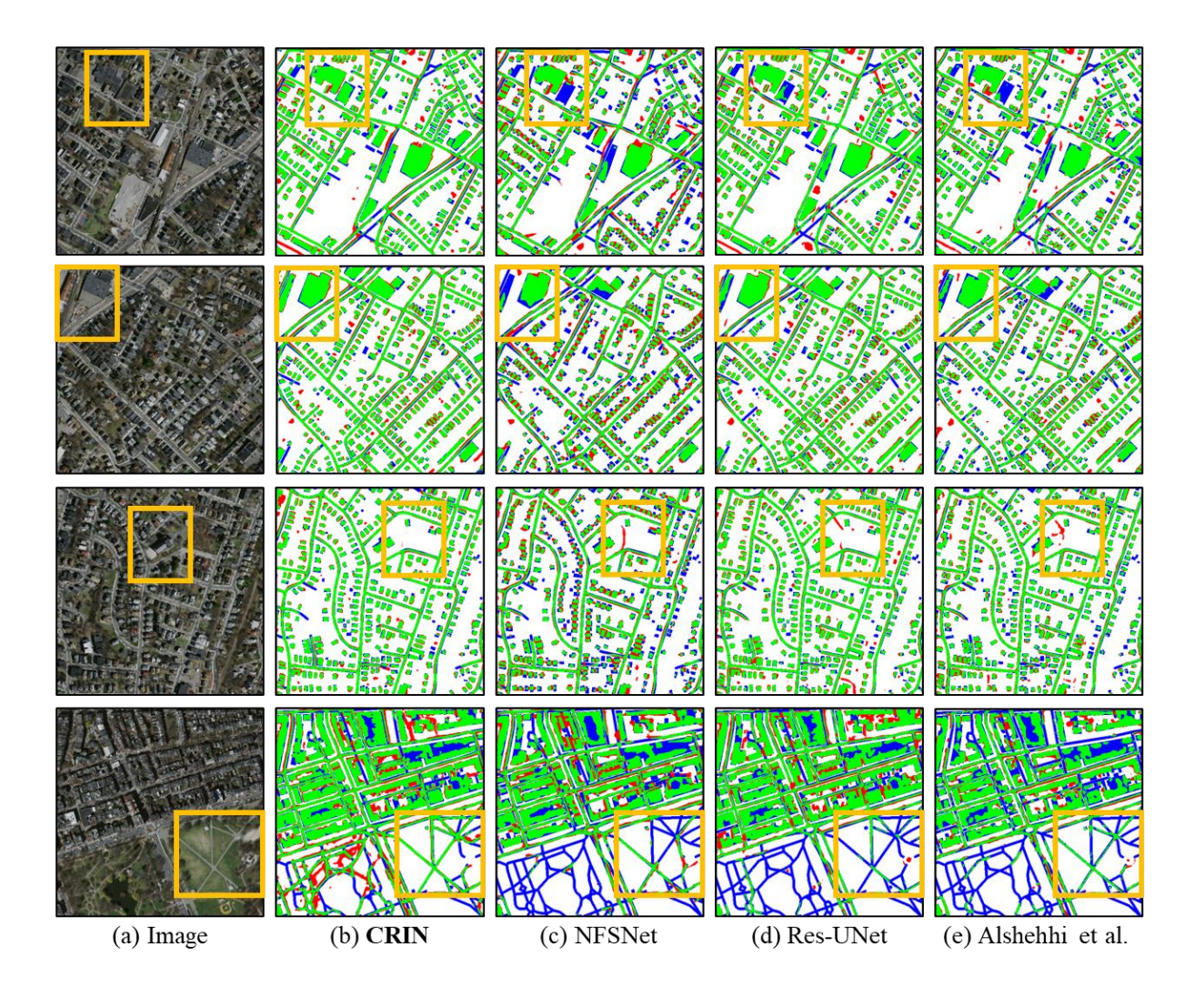


Figure 6. Visualization of the building-road extraction results of the comparison methods in the Massachusetts dataset.

Furthermore, we conducted ablation experiments on the Massachusetts dataset to validate the effectiveness of the proposed modules. We selected the U-Net architecture with the EfficientNet backbone as the baseline. This model is trained and inferred separately on the building and road extraction tasks. From Table 2, we can see that the baseline model achieved the F1-score of 81.85% and 71.03% on building extraction and road extraction tasks. If we simply add multiple classifiers to the baseline and convert it into a multitask model, the accuracy of the road extraction task is improved by 2.14% on the F1-score. However, the model's performance on building extraction is slightly decreased. It demonstrates the 'seesaw

phenomenon' of multitask learning where the road extraction task is improved with the building extraction task sacrificed. This is because the road extraction task becomes dominant in the training process and thus leads to unbalanced learning. If we improve multitask learning by integrating the MTI module, the accuracy of both tasks can be improved by fully utilizing the spatial correlation between buildings and roads. As a result, the F1-score of buildings and roads are improved by 0.6% and 2.28%, respectively. Furthermore, if we utilize the CSI module to learn the optimal reception field for different tasks, the accuracy of both tasks can be improved.

We also present the model complexity in Table 2 using GFlops. The baseline model has the highest complexity because the model is inferred twice to generate the building and road predictions. The complexity of a simple multitask network is appropriate half of the baseline model. It should be noted that the model complexity is obviously decreased with MTI as compared with the multitask model, which is because MTI reduces the computation cost using successive group convolution. Furthermore, CSI slightly increases the computational cost and achieves the best performance on both tasks.

Table 2 Ablation experimental results on the Massachusetts dataset

| Method       | Multitask | MTI | CSI  | Task     | IoU      | Precision | Recall | F1-Score | GFlops   |       |      |
|--------------|-----------|-----|------|----------|----------|-----------|--------|----------|----------|-------|------|
|              |           |     |      | Building | 69.28    | 81.73     | 81.98  | 81.85    | 1.57.7.2 |       |      |
| Baseline     | Baseline  |     |      | Road     | 55.07    | 75.09     | 67.38  | 71.03    | 1.57×2   |       |      |
| Ablation 1 √ | 1         |     |      | Building | 69.16    | 85.19     | 78.62  | 81.77    |          |       |      |
|              |           |     | Road | 57.69    | 76.73    | 69.92     | 73.17  | 1.62     |          |       |      |
| Ablation 2 √ | 1         | 1   |      |          | Building | 70.14     | 85.56  | 79.56    | 82.45    |       |      |
|              | ٧         | V   | Road | 57.86    | 78.65    | 68.65     | 73.31  | 0.91     |          |       |      |
|              | 1         |     |      | ,        |          | Building  | 71.15  | 83.79    | 82.5     | 83.14 | 0.96 |
| Ablation 3   | V         | √   | √    | Road     | 59.09    | 75.49     | 73.12  | 74.29    | 0.90     |       |      |

The intermediate features of the task-specific and task-shared feature space of the MTI module are presented in Figure 7. From Figure 7 (a) and (b) we can see that the task-specific building and road features focus on localizing buildings and roads respectively. Meanwhile, features from the shared feature space focus on capturing the context information and colocation pattern between buildings and roads. The accuracy of buildings and roads can be improved by separating task-specific and task-shared features.

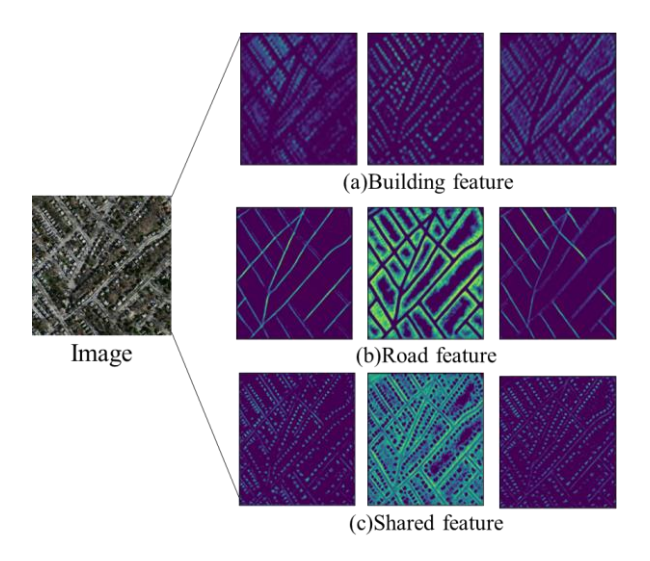


Figure 7. Visualization of the features in the task-specific and task-shared feature spaces.

# **4.3** Experiments on the AIOI dataset

We conducted experiments on another large-scale AIOI dataset. The AIOI dataset includes images and labels from 9 cities that cover various urban and suburban scenes. The comparison methods are trained and evaluated using data from different cities, and thus can testify the models' performance of large-scale mapping in practical scenarios. The quantitative comparison as listed in Table 2 shows that the CRIN model outperformed the comparison models and achieved the highest accuracy in both buildings and roads. The patch-based methods as proposed by Saito et al. and Alshehhi et al. cannot perform well on large-scale mapping because these methods cannot fully utilize the spatial information of VHR remote sensing images. Meanwhile, although limited performance on the Massachusetts dataset,

NFSNet achieves the second highest score on the AIOI dataset, which indicates the performance of NFSNet is influenced by the spatial resolution of images.

The ablation experimental results as shown in Table 3 demonstrate the effectiveness of the proposed MTI and CSI modules. The 'seesaw phenomenon' also leads to an accuracy drop in the building extraction task of the multitask method. The proposed MTI enables balanced learning and thus improves the model accuracy of both tasks. The CSI module further improves the model performance on different tasks by learning the optimal reception field. As a result, our proposed CRIN model improves the F1-score by 3.21% and 3.38% on building and road extraction tasks respectively with less computational cost, demonstrating the model's effectiveness in large-scale and cross-city mapping.

Table 3 Quantitative Comparison with SOTA Methods on the AIOI dataset

| Method          | Type      | Task     | IoU   | Precision | Recall | F1-Score |
|-----------------|-----------|----------|-------|-----------|--------|----------|
| CRIN(ours)      |           | Building | 66.25 | 79.99     | 79.41  | 79.7     |
|                 |           | Road     | 52.22 | 68.98     | 68.25  | 68.61    |
| Saito et al.    |           | Building | 38.02 | 60.24     | 50.75  | 55.09    |
|                 | Multitask | Road     | 18.15 | 35.9      | 26.86  | 30.73    |
| Alshehhi et al. |           | Building | 38.12 | 58.37     | 52.35  | 55.2     |
|                 |           | Road     | 17.93 | 31.96     | 28.99  | 30.4     |
| NFSNet          |           | Building | 60.4  | 77.82     | 72.96  | 75.31    |
|                 |           | Road     | 48.11 | 70.24     | 60.42  | 64.96    |
| JointNet        |           | Building | 47.5  | 71.74     | 58.43  | 64.41    |
|                 |           | Road     | 30.27 | 56.07     | 39.67  | 46.47    |
| MCG-UNet        |           | Building | 51.27 | 76.12     | 61.1   | 67.79    |
|                 | Separate  | Road     | 38.3  | 67.25     | 47.08  | 55.38    |
| Res-U-Net       | -         | Building | 57.07 | 77.21     | 68.63  | 72.67    |
|                 |           | Road     | 47.2  | 71.06     | 58.43  | 64.13    |
| Mnih et al.     |           | Building | 37.48 | 67.88     | 45.55  | 54.52    |
|                 |           | Road     | 21.99 | 33.73     | 38.73  | 36.06    |

Table 4 Ablation experimental results on the AIOI dataset

| Method     | Multitask | MTI          | CSI |          | IoU      | Precision | Recall | F1-Score | GFlops  |      |
|------------|-----------|--------------|-----|----------|----------|-----------|--------|----------|---------|------|
|            |           |              |     | Building | 61.93    | 79.21     | 73.95  | 76.49    | 1.57.70 |      |
| Baseline   |           |              |     | Road     | 48.4     | 66.37     | 64.13  | 65.23    | 1.57×2  |      |
| Ablation 1 | ,         |              |     | Building | 60.65    | 79.51     | 71.88  | 75.5     |         |      |
|            | V         |              |     | Road     | 48.8     | 67.05     | 64.2   | 65.59    | 1.62    |      |
| Ablation 2 | ,         | ,            |     | Building | 62.93    | 80.04     | 74.64  | 77.25    |         |      |
|            | $\sqrt{}$ | <b>V</b>     |     | Road     | 49.52    | 65.99     | 66.48  | 66.24    | 0.91    |      |
| Ablation 3 |           | <b>V V V</b> |     | ,        | Building | 66.25     | 79.99  | 79.41    | 79.7    | 0.06 |
|            | √         |              | V   | Road     | 52.22    | 68.98     | 68.25  | 68.61    | 0.96    |      |

We visualize the large-scale mapping results of different cities in Figure 8, including Atlanta, New York, and New Heaven. From Figure 8 we can see that CRIN obtains the best qualitative visualization results as compared to the other methods. The buildings and roads are seriously omitted by the patch-based method. Meanwhile, some buildings and roads as predicted by NFSNet and Res-UNet are incomplete and discontinuous. On the contrary, CRIN successfully depicts the buildings and roads by taking advantage of the complementary between buildings and roads. CRIN also outperforms the comparison methods by precisely depicting buildings and roads from complex urban blocks, as shown in Figure 8 row 3.

# • Atlanta • New York • New Heaven

Figure 8. Visualization of the building and road extraction results on the AIOI dataset.

(b) CRIN

# 5. Discussion

(a) Image

In this section, we will discuss and compare the complexity of models, visualize, and analyze whether different tasks rely on the same model reception field, apply the proposed modules to other backbone networks, and discuss the limitation of our proposed method.

(c) NFSNet

(d) Res-UNet

(e) Alshehhi et al.

# **5.1 Model Complexity**

Apart from model accuracy and generalization ability, the complexity of models also matters in practical applications. In particular, the number of parameters and flops reflects the computational cost of the model in the inference stage; the frame per second (FPS) index indicates the time used for inference. Table 5 shows the number of parameters, flops, and FPS of each model testified on a single RTX 3090 GPU. In general, the separate models infer slower than the multitask model with higher Flops and lower FPS since these models are trained

separately on roads and buildings, and need to be inferred twice to obtain buildings and roads prediction. As a result, the number of flops and parameters is doubled as compared to the single model. The Flops of Joint-Net and MCG-UNet are rather high since these methods maintain high feature resolution with multiple channels in the model, which lead to high computational cost. Among the multitask methods, the proposed CRIN obtain the lowest flops and the second highest FPS, which indicates the low computational cost and high inferring speed of our proposed methods. In comparison, the methods proposed by Saito et al. and Alshehhi et al. are much slower by approximately inferring a single 512x512 image per second. The reason is twofold. These patch-based methods receive 64x64 image patches as the input, and clipping these image patches with a stride of 16x16 leads to multiple inferring times as compared with the FCN-based methods. Moreover, to capture context information, these patch-based methods require input patches that are 4-time larger than the output prediction, resulting in redundant computation in the inference stage. In comparison, the FCN-based CRIN and NFS-Net are faster than not only the separate methods but also the patch-based methods. However, despite high FPS, NFSNet is prone to omit small buildings and slim roads since the predictions are generated from very low-resolution features (16 times lower than the input image). CRIN, on the contrary, can well balance computation cost, inference speed, and accuracy.

Table 5 Model complexity of the comparison methods

| Method          | Type      | GFlops | Parameters | FPS   |
|-----------------|-----------|--------|------------|-------|
| CRIN            |           | 0.96   | 4.38       | 38.51 |
| Saito et al.    | Multitask | 144.27 | 2.42       | 1.02  |
| Alshehhi et al. | Mulittask | 41.8   | 19.45      | 1.59  |
| NFSNet          |           | 9.82   | 11.91      | 63.3  |
| Joint-Net       |           | 417.93 | 8.84       | 9.52  |
| MCG-UNet        | Separate  | 1325   | 55.78      | 7.68  |
| Res-U-Net       |           | 83.74  | 50.2       | 28.85 |
|                 | Separate  |        |            |       |

Mnih et al. 79.31 34.71 0.6

### 5.2 Scale contribution

In the proposed CSI module, multiple branches are designed to extract features by different reception field, including skip connection, 7x7, 11x11, and 21x21; a scale attention module then determines the contribution of each scale, and fuse the features based on the attention value. The CSI module can determine the optimal reception field for each task by applying argmax operation to each channel in building features and road features. Moreover, the CSI module is integrated into different stages of the decoder module and can determine the optimal reception field at different feature resolutions. A question arises: do building and road extraction tasks rely differently on the model reception field and how?

In Figure 9, we visualize the optimal receptive field for building extraction and road extraction tasks on different feature resolutions and datasets. From Figure (a), we can see that the optimal reception field for buildings and roads is similar, with most features remaining the original reception field by skip connection, and some features select large convolution kernels such as 11x11 and 21x21 as the optimal reception fields. It indicates that the high-level feature presentations for buildings and roads rely similarly on the model reception field. However, as the feature resolution increases, the optimal feature reception field for different tasks differs. More specifically, the building extraction task relies more on smaller reception fields such as skip connection, and 7X7; the road extraction task relies heavier on large reception fields such as 21x21 and 11x11 than the building extraction task. This is probably because roads are objects of linear shapes and depend on the consistency of shape and position. As a result, fusing shallow features from the encoder network plays an important role in recovering spatial information(Zhang and Wang, 2019) and thus the optimal reception field of the road extraction task is larger to perceive and recover spatial information from high-resolution features. From Figure (b) we can see that the optimal receptive field 21x21 for road extraction appears in the

4x resolution scale, which is 2 times lower than the Massachusetts dataset. Considering that the spatial resolution of the Massachusetts dataset is approximately 3 times lower than the AIOI dataset, we suppose that the optimal reception field of different tasks is related not only to the depth of the decoder network but also the image spatial resolution. Designing (or searching) the optimal network architecture for different network scales or feature resolutions is an interesting question to be solved.

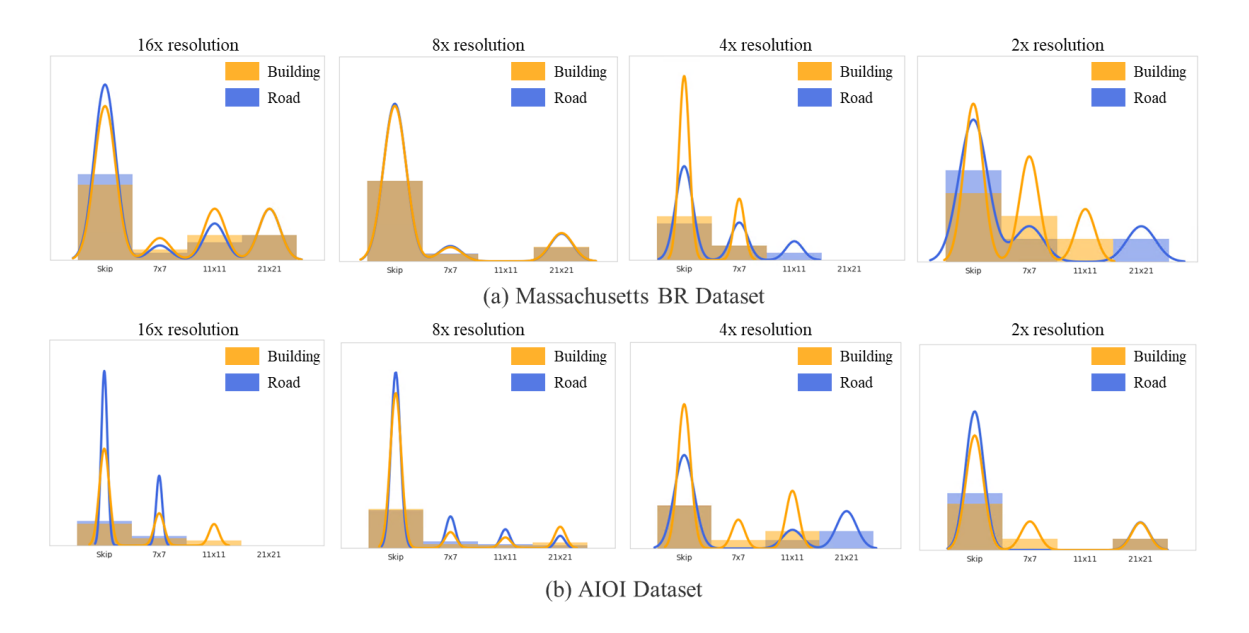


Figure 9. The contribution of different scales on different feature resolutions and datasets.

# **5.3** Application to other backbones

In this study, we selected Efficient Net as the backbone, which is an effective architecture searched from millions of large-scale images and labels. To demonstrate the lightweight advantage of CRIN, we select the EfficientNet-b0 as the backbone network. In fact, CRIN can also be applied to various backbone networks, such as EffecientNet-b7(Tan and Le, 2020), ResNet(He et al., 2015), and ConvNext(Liu et al., 2022). As shown in Table 7, the model performance of CRIN can be applied to other backbone networks such as EfficientNet-b7 and increase the mapping accuracy of building-road collaborative extraction. Despite the better performance, these backbone networks improve the model complexity as compared to the

EffecientNet-b0 network applied in CRIN. In conclusion, the proposed CRIN model can well balance between model accuracy and complexity.

Table 6 Experimentation results on different backbones

| Method          | Dataset         | Task     | IoU  | Precision | Recall | F1-Score |
|-----------------|-----------------|----------|--|-----------|--------|----------|
|                 |                 | Building | 70.5   | 83.99     | 81.45  | 82.7     |
| ResNet 34       |                 | Road     | 58.32  | 77.53     | 70.19  | 73.68    |
|                 |                 | Building | 70.51  | 86.95     | 78.85  | 82.7     |
| ConvNext.       | Massachusetts - | Road     | 61.15  | 77.7      | 74.16  | 75.89    |
|                 |                 | Building | 73.89  | 86        | 84     | 84.99    |
| EfficientNet-b7 |                 | Road     | 62.62  | 78.25     | 75.83  | 77.02    |
|                 |                 | Building | 59.51  | 79.58     | 70.24  | 74.62    |
| ResNet 34       |                 | Road     | 49.5   | 70.38     | 62.53  | 66.22    |
|                 |                 | Building | 56.91  | 81.91     | 65.09  | 72.54    |
| ConvNext        | AIOI<br>-       | Road     | 46.28  | 66.47     | 60.38  | 63.28    |
|                 |                 | Building | 69.61  | 82.12     | 82.05  | 82.08    |
| EfficientNet-b7 |                 | Road     | ilding 59.51 79.58 70.38 60 60.47 60 60.61 82.12 8 | 69.52     | 71.98  |          |

# 6. Conclusion

Buildings and roads are the two most basic man-made environments that carry and interconnect our society. The geodata of buildings and roads are valuable for various frontier applications. However, many existing extraction methods ignore the strong spatial correlation between roads and buildings and extract buildings and roads from remote sensing images in isolation. Meanwhile, some multitask methods cause the "seesaw phenomenon" where the accuracy of one task is improved by hurting the performance of another task, which is demonstrated in our experiments. To tackle these problems, we propose a building-road collaborative extraction method by introducing inner-task, cross-task, and cross-scale feature interaction. The features are projected into task-specific and task-shared feature spaces and thus promote cross-task interaction while preserving the information from each task. Furthermore, a cross-scale interaction module is proposed to automatically learn and select the optimal reception field for each feature space, and thus exploit optimal feature representations for each

specific task. As compared with the existing methods, our proposed collaborative extraction method can output both the building and road prediction results, improve the inference speed, and enhance the multi-task recognition accuracy through the proposed cross-task and cross-scale feature interaction. Experimental results on two large-scale datasets show that our proposed algorithm can achieve robust and rapid building-road collaborative extraction with strong generalization performance and high extraction accuracy, showing great potential in large-scale mapping.

Although our proposed method achieves better accuracy than the comparison methods, the model performance can be further improved by considering the noise contained in the ground truth label. Since many existing datasets are developed from the crowdsource data such as OSM, the labels are usually not strictly aligned with the image, which affects model learning. We will further explore noisy label learning to achieve more robust building-road collaborative extraction.

### References

- Abdollahi, A., Pradhan, B., Shukla, N., Chakraborty, S., Alamri, A., 2021. Multi-Object Segmentation in Complex Urban Scenes from High-Resolution Remote Sensing Data. Remote Sensing 13, 3710. https://doi.org/10.3390/rs13183710
- Adriano, B., Yokoya, N., Xia, J., Miura, H., Liu, W., Matsuoka, M., Koshimura, S., 2021. Learning from multimodal and multitemporal earth observation data for building damage mapping. ISPRS Journal of Photogrammetry and Remote Sensing 175, 132–143. https://doi.org/10.1016/j.isprsjprs.2021.02.016
- Alshehhi, R., Marpu, P.R., Woon, W.L., Mura, M.D., 2017. Simultaneous extraction of roads and buildings in remote sensing imagery with convolutional neural networks. ISPRS Journal of Photogrammetry and Remote Sensing 130, 139–149. https://doi.org/10.1016/j.isprsjprs.2017.05.002
- Awrangjeb, M., Zhang, C., Fraser, C., 2013. Improved building detection using texture information. ISPRS International Archives of the Photogrammetry, Remote Sensing and Spatial Information Sciences XXXVIII-3/W22. https://doi.org/10.5194/isprsarchives-XXXVIII-3-W22-143-2011
- Ayala, C., Aranda, C., Galar, M., 2021a. Multi-Class Strategies for Joint Building Footprint and Road Detection in Remote Sensing. Applied Sciences 11, 8340. https://doi.org/10.3390/app11188340

- Ayala, C., Sesma, R., Aranda, C., Galar, M., 2021b. A Deep Learning Approach to an Enhanced Building Footprint and Road Detection in High-Resolution Satellite Imagery. Remote Sensing 13, 3135. https://doi.org/10.3390/rs13163135
- Bai, B., Fu, W., Lu, T., Li, S., 2022. Edge-Guided Recurrent Convolutional Neural Network for Multitemporal Remote Sensing Image Building Change Detection. IEEE Transactions on Geoscience and Remote Sensing 60, 1–13. https://doi.org/10.1109/TGRS.2021.3106697
- Belli, D., Kipf, T., 2019. Image-conditioned graph generation for road network extraction. arXiv preprint arXiv:1910.14388.
- Bouziani, M., Goïta, K., He, D.-C., 2010. Automatic change detection of buildings in urban environment from very high spatial resolution images using existing geodatabase and prior knowledge. ISPRS Journal of Photogrammetry and Remote Sensing 65, 143–153. https://doi.org/10.1016/j.isprsjprs.2009.10.002
- Bradbury, K., Brigman, B., Collins, L., Johnson, T., Lin, S., Newell, R., Park, S., Sunith Suresh, Hoel Wiesner, Xi, Y., 2016. Aerial imagery object identification dataset for building and road detection, and building height estimation. https://doi.org/10.6084/M9.FIGSHARE.C.3290519.V1
- Crew, B., 2021. Sustainable Development Goals research speaks to city strengths and priorities. Nature. https://doi.org/10.1038/d41586-021-02405-w
- Ding, C., Weng, L., Xia, M., Lin, H., 2021. Non-Local Feature Search Network for Building and Road Segmentation of Remote Sensing Image. ISPRS International Journal of Geo-Information 10, 245. https://doi.org/10.3390/ijgi10040245
- Fleischmann, M., Arribas-Bel, D., 2022. Geographical characterisation of British urban form and function using the spatial signatures framework. Sci Data 9, 546. https://doi.org/10.1038/s41597-022-01640-8
- Ghanea, M., Moallem, P., Momeni, M., 2016. Building extraction from high-resolution satellite images in urban areas: recent methods and strategies against significant challenges. International Journal of Remote Sensing 37, 5234–5248. https://doi.org/10.1080/01431161.2016.1230287
- Griffiths, D., Boehm, J., 2019. Improving public data for building segmentation from Convolutional Neural Networks (CNNs) for fused airborne lidar and image data using active contours. ISPRS Journal of Photogrammetry and Remote Sensing 154, 70–83. https://doi.org/10.1016/j.isprsjprs.2019.05.013
- Guo, H., Shi, Q., Du, B., Zhang, L., Wang, D., Ding, H., 2021a. Scene-Driven Multitask Parallel Attention Network for Building Extraction in High-Resolution Remote Sensing Images. IEEE Transactions on Geoscience and Remote Sensing 59, 4287–4306. https://doi.org/10.1109/TGRS.2020.3014312
- Guo, H., Shi, Q., Marinoni, A., Du, B., Zhang, L., 2021b. Deep building footprint update network: A semi-supervised method for updating existing building footprint from bi-temporal remote sensing images. Remote Sensing of Environment 264, 112589. https://doi.org/10.1016/j.rse.2021.112589
- Guo, H., Su, X., Tang, S., Du, B., Zhang, L., 2021c. Scale-Robust Deep-Supervision Network for Mapping Building Footprints from High-Resolution Remote Sensing Images. IEEE J. Sel. Top. Appl. Earth Observations Remote Sensing 1–1. https://doi.org/10.1109/JSTARS.2021.3109237
- He, K., Zhang, X., Ren, S., Sun, J., 2015. Deep Residual Learning for Image Recognition. arXiv:1512.03385 [cs].
- Huang, X., Cao, Y., Li, J., 2020. An automatic change detection method for monitoring newly constructed building areas using time-series multi-view high-resolution optical satellite images. Remote Sensing of Environment 244, 111802. https://doi.org/10.1016/j.rse.2020.111802
- Huang, X., Zhang, L., 2011. A Multidirectional and Multiscale Morphological Index for Automatic Building Extraction from Multispectral GeoEye-1 Imagery. photogramm eng remote sensing 77, 721–732. https://doi.org/10.14358/PERS.77.7.721

- Huang, X., Zhang, L., 2009. Road centreline extraction from high-resolution imagery based on multiscale structural features and support vector machines. International Journal of Remote Sensing 30, 1977–1987. https://doi.org/10.1080/01431160802546837
- Ji, S., Wei, S., Lu, M., 2019. Fully Convolutional Networks for Multisource Building Extraction From an Open Aerial and Satellite Imagery Data Set. IEEE Transactions on Geoscience and Remote Sensing 57, 574–586. https://doi.org/10.1109/TGRS.2018.2858817
- Kingma, D.P., Ba, J., 2017. Adam: A Method for Stochastic Optimization. arXiv:1412.6980 [cs].
- Krizhevsky, A., Sutskever, I., Hinton, G.E., 2017. ImageNet classification with deep convolutional neural networks. Commun. ACM 60, 84–90. https://doi.org/10.1145/3065386
- Laurance, W.F., Clements, G.R., Sloan, S., O'Connell, C.S., Mueller, N.D., Goosem, M., Venter, O., Edwards, D.P., Phalan, B., Balmford, A., Van Der Ree, R., Arrea, I.B., 2014. A global strategy for road building. Nature 513, 229–232. https://doi.org/10.1038/nature13717
- LI, D., SHAN, J., SHAO, Z., ZHOU, X., YAO, Y., 2013. Geomatics for Smart Cities Concept, Key Techniques, and Applications. Geo-spatial Information Science 16, 13–24. https://doi.org/10.1080/10095020.2013.772803
- Lian, R., Wang, W., Mustafa, N., Huang, L., 2020. Road Extraction Methods in High-Resolution Remote Sensing Images: A Comprehensive Review. IEEE Journal of Selected Topics in Applied Earth Observations and Remote Sensing 13, 5489–5507. https://doi.org/10.1109/JSTARS.2020.3023549
- Liu, Y., Chen, D., Ma, A., Zhong, Y., Fang, F., Xu, K., 2021. Multiscale U-Shaped CNN Building Instance Extraction Framework With Edge Constraint for High-Spatial-Resolution Remote Sensing Imagery. IEEE Transactions on Geoscience and Remote Sensing 59, 6106–6120. https://doi.org/10.1109/TGRS.2020.3022410
- Liu, Y., Fan, B., Wang, L., Bai, J., Xiang, S., Pan, C., 2018. Semantic labeling in very high resolution images via a self-cascaded convolutional neural network. ISPRS Journal of Photogrammetry and Remote Sensing, Deep Learning RS Data 145, 78–95. https://doi.org/10.1016/j.isprsjprs.2017.12.007
- Liu, Z., Mao, H., Wu, C.-Y., Feichtenhofer, C., Darrell, T., Xie, S., 2022. A ConvNet for the 2020s. https://doi.org/10.48550/arXiv.2201.03545
- Long, J., Shelhamer, E., Darrell, T., 2015. Fully convolutional networks for semantic segmentation, in: 2015 IEEE Conference on Computer Vision and Pattern Recognition (CVPR). Presented at the 2015 IEEE Conference on Computer Vision and Pattern Recognition (CVPR), IEEE, Boston, MA, USA, pp. 3431–3440. https://doi.org/10.1109/CVPR.2015.7298965
- Lu, X., Zhong, Y., Zheng, Z., Liu, Y., Zhao, J., Ma, A., Yang, J., 2019. Multi-Scale and Multi-Task Deep Learning Framework for Automatic Road Extraction. IEEE Trans. Geosci. Remote Sensing 57, 9362–9377. https://doi.org/10.1109/TGRS.2019.2926397
- Lu, X., Zhong, Y., Zheng, Z., Zhang, L., 2021. GAMSNet: Globally aware road detection network with multi-scale residual learning. ISPRS Journal of Photogrammetry and Remote Sensing 175, 340–352. https://doi.org/10.1016/j.isprsjprs.2021.03.008
- Mnih, Volodymyr, n.d. Machine Learning for Aerial Image Labeling.
- Ok, A.O., Senaras, C., Yuksel, B., 2013. Automated Detection of Arbitrarily Shaped Buildings in Complex Environments From Monocular VHR Optical Satellite Imagery. IEEE Transactions on Geoscience and Remote Sensing 51, 1701–1717. https://doi.org/10.1109/TGRS.2012.2207123
- Ronneberger, O., Fischer, P., Brox, T., 2015. U-Net: Convolutional Networks for Biomedical Image Segmentation, in: Navab, N., Hornegger, J., Wells, W.M., Frangi, A.F. (Eds.), Medical Image Computing and Computer-Assisted Intervention MICCAI 2015, Lecture Notes in Computer Science. Springer International Publishing, Cham, pp. 234–241. https://doi.org/10.1007/978-3-319-24574-4\_28
- Saito, S., Yamashita, Y., Aoki, Y., 2016. Multiple Object Extraction from Aerial Imagery with Convolutional Neural Networks. Journal of Imaging Science and Technology 60, 10402–1/10402. https://doi.org/10.2352/J.ImagingSci.Technol.2016.60.1.010402
- Seppke, B., Dreschler-Fischer, L., Wilms, C., 2016. Robust Superpixel Based Segmentation for Urbanization Monitoring by Means of Spectral Remote Sensing Images, in: DLT DGPF Symposium.

- Shao, Z., Tang, P., Wang, Z., Saleem, N., Yam, S., Sommai, C., 2020. BRRNet: A Fully Convolutional Neural Network for Automatic Building Extraction From High-Resolution Remote Sensing Images. Remote Sensing 12, 1050. https://doi.org/10.3390/rs12061050
- Tan, M., Le, Q.V., 2020. EfficientNet: Rethinking Model Scaling for Convolutional Neural Networks. arXiv:1905.11946 [cs, stat].
- Tang, H., Liu, J., Zhao, M., Gong, X., 2020. Progressive Layered Extraction (PLE): A Novel Multi-Task Learning (MTL) Model for Personalized Recommendations, in: Proceedings of the 14th ACM Conference on Recommender Systems, RecSys '20. Association for Computing Machinery, New York, NY, USA, pp. 269–278. https://doi.org/10.1145/3383313.3412236
- Xu, Y., Wu, L., Xie, Z., Chen, Z., 2018. Building Extraction in Very High Resolution Remote Sensing Imagery Using Deep Learning and Guided Filters. Remote Sensing 10, 144. https://doi.org/10.3390/rs10010144
- Yager, N., Sowmya, A., 2003. Support Vector Machines for Road Extraction from Remotely Sensed Images. https://doi.org/10.1007/978-3-540-45179-2\_36
- Zha, Y., Gao, J., Ni, S., 2003. Use of normalized difference built-up index in automatically mapping urban areas from TM imagery. International Journal of Remote Sensing 24, 583–594. https://doi.org/10.1080/01431160304987
- Zhang, Z., Wang, Y., 2019. JointNet: A Common Neural Network for Road and Building Extraction. Remote Sensing 11, 696. https://doi.org/10.3390/rs11060696
- Zhou, L., Zhang, C., Wu, M., 2018. D-LinkNet: LinkNet with Pretrained Encoder and Dilated Convolution for High Resolution Satellite Imagery Road Extraction, in: 2018 IEEE/CVF Conference on Computer Vision and Pattern Recognition Workshops (CVPRW). Presented at the 2018 IEEE/CVF Conference on Computer Vision and Pattern Recognition Workshops (CVPRW), pp. 192–1924. https://doi.org/10.1109/CVPRW.2018.00034
- Zhu, Q., Liao, C., Hu, H., Mei, X., Li, H., 2020. MAP-Net: Multiple Attending Path Neural Network for Building Footprint Extraction From Remote Sensed Imagery. IEEE Transactions on Geoscience and Remote Sensing 1–13. https://doi.org/10.1109/TGRS.2020.3026051
- Zhu, X.X., Tuia, D., Mou, L., Xia, G.-S., Zhang, L., Xu, F., Fraundorfer, F., 2017. Deep Learning in Remote Sensing: A Comprehensive Review and List of Resources. IEEE Geoscience and Remote Sensing Magazine 5, 8–36. https://doi.org/10.1109/MGRS.2017.2762307